Crustal structure in southeastern Egypt: Symmetric thinning of the northern Red Sea rifted margins

Ahmed Hosny[1]* and Andrew Nyblade[2]*
[1]Seismology Department, National Research Institute of Astronomy and Geophysics (NRIAG), Helwan, Cairo, Egypt
[2]Department of Geosciences, Pennsylvania State University, University Park, Pennsylvania 16802, USA

ABSTRACT

Crustal structure in southeastern Egypt has been investigated to elucidate the nature of crustal thinning across the northern Red Sea. P-wave receiver function modeling for 7 stations in southeastern Egypt yields typical Proterozoic crustal thicknesses of 35–38 km around Lake Aswan, and thinner crust (25–26 km) within 50 km of the Red Sea coast. The Vp/Vs ratios are on average 1.78 and indicate an intermediate-composition crust. These results, when combined with other estimates of crustal thickness in the region, reveal a symmetric pattern of crustal thickness beneath the conjugate margins of the northern Red Sea. Such a pattern is consistent with a pure shear model of extension, and suggests that the greater amounts of uplift and volcanism on the eastern side of the Red Sea compared to the western side may be the result of deeper flow in the mantle associated with the African superplume and not a direct consequence of the rifting process.

INTRODUCTION

The nature of crustal extension across the Red Sea Rift, long regarded as one of the best locations to investigate continental breakup, has been debated in studies for more than 30 years (e.g., Cochran, 1983, 2005; Voggenreiter et al., 1988; Bohannon, 1989; Dixon et al., 1989; Rihm et al., 1991). Asymmetric structure across the rift, inferred from seismic refraction profiles (e.g., Gaulier et al., 1988; Egloff et al., 1991; Voggenreiter et al., 1988; Rihm et al., 1991) and the greater amounts of Cenozoic volcanism and uplift along the eastern side of the Red Sea, have been used to argue for extension via simple shear (Fig. 1A) (e.g., Voggenreiter et al., 1988; Bohannon, 1989; Dixon et al., 1989; Rihm et al., 1991). Interpretations of asymmetric crustal structure have also been used to support a pull-apart model of the northern Red Sea with oblique extension along strike-slip faults (Makris and Rihm, 1991). In contrast, the seismic images of crustal structure have been used to argue for symmetric structure across the northern Red Sea and pure shear extension by diffuse ductile flow below block faulting in the uppermost crust (Fig. 1B) (e.g., Cochran, 1983, 2005; Martinez and Cochran, 1988). As these models all derive from interpretations of the same seismic data, new constraints on crustal structure across the Red Sea margins are necessary to evaluate them and advance our understanding of how the rifted crust has been extended.

Here we present new estimates of crustal thickness from southeastern Egypt, using P-wave receiver functions obtained from broadband seismograms recorded on the Egyptian National Seismic Network, that when combined with previous estimates of crustal thickness reveal a symmetric pattern of crustal thickness beneath the northern Red Sea conjugate margins. This finding supports a pure shear model of extension, and suggests that the greater amounts of uplift and volcanism on the eastern side of the Red Sea compared to the western side may be the result of deeper flow in the mantle associated with the African superplume, and not a direct consequence of the rifting process.

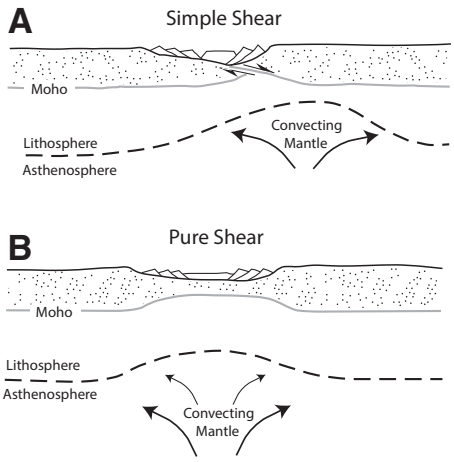

Figure 1. A: Simple shear model. B: Pure shear rift model. Models redrawn from Dixon et al. (1989).

BACKGROUND

The Red Sea Rift formed by the rupturing of Proterozoic lithosphere starting in the Late Oligocene. Seafloor spreading began ca. 5 Ma in the southern Red Sea, and in the central and northern Red Sea the transition from continental to oceanic rifting is ongoing (Martinez and Cochran, 1988; Cochran et al., 1991). The Gulf of Suez to the northwest of the Red Sea was part of the Red Sea until it was cut off by the development of the Dead Sea transform in the Middle Miocene.

Uplift and unroofing began along the entire Red Sea at ca. 34 Ma (Omar and Steckler, 1995), well before the onset of rifting, and Proterozoic basement is exposed on both sides of the rift (Fig. 2). Flood basalt volcanism in the southern Red Sea region (Ethiopia and Yemen) occurred at ca. 30 Ma (Coulié et al., 2003), dike intrusion along the entire length of the Red Sea on the Arabian side occurred between 24 and 21 Ma

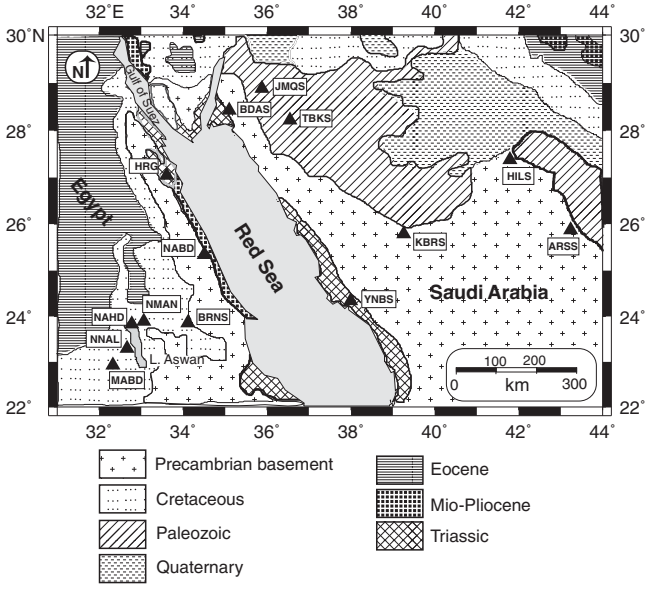

Figure 2. Simplified geological map of regions surrounding northern Red Sea. Black triangles show seismic station locations. Mio—Miocene.

*E-mails: aha13@psu.edu; nyblade@psu.edu.

(Sebai et al., 1991; Bosworth et al., 2005), and episodic volcanism has occurred to the present in the Afar, southern Yemen, and the Harrats region of the Arabian shield. Along the Egyptian Red Sea coast, minor basaltic flows and dikes are found in the lowermost synrift units (Bosworth et al., 2005), but rifting in the northern Red Sea has been largely amagmatic over most of its development.

The morphology of the northern Red Sea is characterized by abrupt continental margins, narrow coastal shelves and plains, and a broader main trough. Extension in the upper crust has been primarily accommodated by block rotation (Cochran et al., 1991; Bosworth et al., 2005), and along-axis segmentation is well developed.

Seismic refraction profiles in the northern Red Sea indicate a crustal thickness of ~20 km beneath the coast on both sides of the rift, with unrifted crustal thickness of ≥~30 km well inland from the coast (Makris et al., 1983; Rihm et al., 1991; Voggenreiter et al., 1988, and references therein), similar to estimates of crustal thickness derived from modeling gravity data (Prutkin and Saleh, 2009). P-wave receiver function estimates of crustal thickness in the Arabian shield are ~35–40 km (Al-Damegh et al., 2005), and estimates of crustal thickness within the center of the northern Red Sea Rift range from ~10 to 15 km (Gaulier et al., 1988).

DATA AND METHODS

Since 2009, the Egyptian National Research Institute of Astronomy and Geophysics has been upgrading the Egyptian National Seismic Network with broadband seismometers. Data from 7 stations located in southeastern Egypt that have been in operation for 1 yr have been used for this study (Fig. 2); the stations are equipped with Nanometrics Trillium 40 or 240 sensors and Trident digitizers recording at 200 samples per second.

We have used data from seismic sources located at epicentral distances between 30° and 90° and with moment magnitude >5.5 for computing receiver functions (see Table DR1 in the GSA Data Repository[1]). The data were detrended, tapered, and band-pass filtered between 0.05 and 8 Hz to remove low-frequency noise and to avoid aliasing, before being decimated to 10 samples/s. The horizontal seismograms were then rotated into the great circle path to obtain the radial and transverse components, and the iterative time-domain deconvolution method of Ligorría and Ammon (1999) was employed to compute the receiver functions using a Gaussian filter width of 1.0 (f < 0.5 Hz) and 500 iterations.

[1]GSA Data Repository item 2014075, Table DR1 (list of events) and Figure DR1 (*H*-κ stack of receiver functions), is available online at www.geosociety.org/pubs/ft2014.htm, or on request from editing@geosociety.org or Documents Secretary, GSA, P.O. Box 9140, Boulder, CO 80301, USA.

TABLE 1. ESTIMATES OF CRUSTAL THICKNESS FROM P-WAVE RECEIVER FUNCTIONS

Station	Lat. (°N)	Long. (°E)	Elevation (m)	Crustal thickness (km)*	Overall uncertainty (km)	Vp/Vs	*N*†
HRG	27.0517	33.6081	227	25.6 ± 1.0	±1.8	1.73 ± 0.06	16
NABD	25.3405	34.5021	298	25.4 ± 0.8	±1.5	1.88 ± 0.05	23
BRNS	23.8559	34.1143	332	27.2 ± 1.7	±2.6	1.72 ± 0.05	13
NMAN	23.9169	33.0749	100	35.7 ± 0.9	±2.2	1.72 ± 0.04	23
NAHD	23.8022	32.7780	100	37.9 ± 1.1	±2.4	1.70 ± 0.07	21
NNAL	23.2931	32.6647	100	34.7 ± 1.9	±3.4	1.85 ± 0.07	12
MABD	22.9226	32.3258	280	35.7 ± 0.7	±2.0	1.85 ± 0.04	12

*From *H*-κ (Vp/Vs = κ; *H* = crustal thickness) stacking using a mean crustal Vp of 6.3 km/s.
†*N* = number of receiver functions used.

To evaluate the quality of the deconvolved traces, a least-squares-misfit criterion was utilized in which the radial waveform for each receiver function is reconstructed by convolving the receiver function back with the corresponding vertical waveform and comparing it with the original radial waveform. Only receiver functions that were recovered at an 85% level or higher were further considered for analysis (Ligorría and Ammon, 1999).

The P-wave receiver functions were modeled using the *H*-κ stacking technique of Zhu and Kanamori (2000) to estimate crustal thickness (*H*) and the crustal Vp/Vs ratio (κ). The stacking procedure transforms the receiver function waveforms from the time-amplitude domain into the *H*-κ parameter space through a weighted sum along theoretical phase moveout curves obtained for given values of *H* and κ and an assumed value of P-wave velocity. The weighted sum (*s*) is given by:

$$s(H, \kappa) = \sum_{j=1}^{N} w_1 r_j(t_1) + w_2 r_j(t_2) - w_3 r_j(t_3), \quad (1)$$

where w_1, w_2, and w_3 are the *a priori* weights for the Ps, PpPs, and PsPs + PpSs phases, respectively, with summation equal to 1; $r_j(t_i)$, i = 1, 2, 3 are the receiver function amplitude values for the jth receiver function at the predicted arrival times t_i; and *N* is the number of receiver functions used.

In applying the *H*-κ technique, it is necessary to select weights w_1, w_2, and w_3 (Equation 1). Although the choice for weights is somewhat subjective, we give more weight to the phases that are most clearly observed and less weight to phases that are not clearly identified or inconsistent among receiver functions. For all stations,

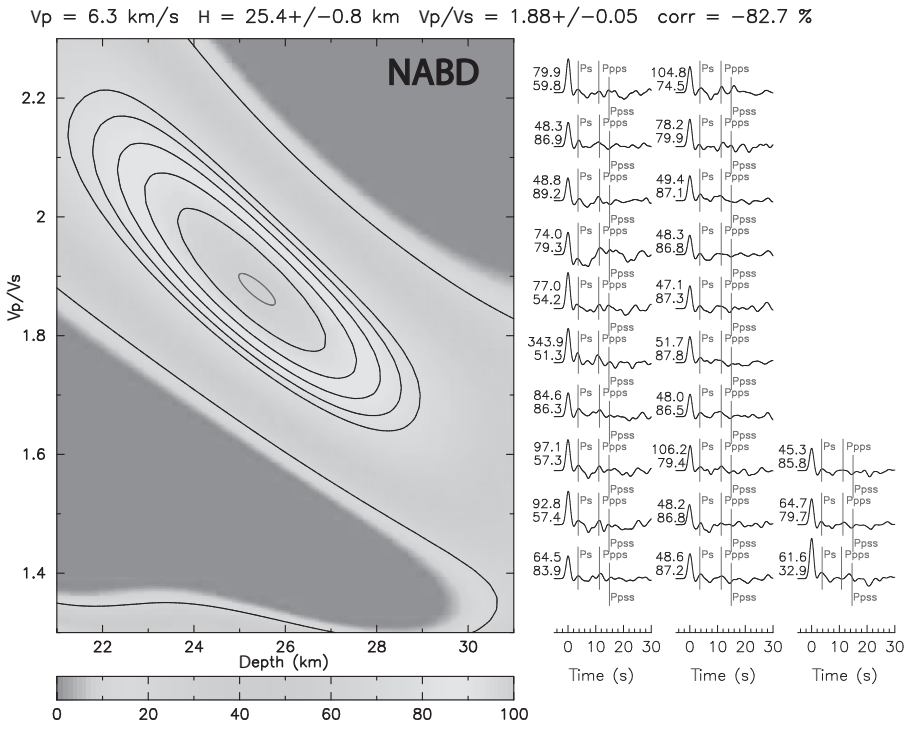

Figure 3. *H*-κ (*H*—crustal thickness; κ—Vp/Vs) stack of receiver functions for station NABD. To left of each receiver function, top number gives event azimuth and bottom number gives event distance in degrees. Contours map out percentage values of objective function given in text.

the first two phases, Ps and PpPs, were clearly seen in the receiver functions, and so each was assigned a weight of 0.4. The PsPs + PpSs phase is not as clear on many of the receiver functions, and therefore it was assigned a weight of 0.2. An average crustal P-wave velocity of 6.3 km/s was used for the stacking, which is between the global average crustal value of 6.45 km/s and the average value of 6.2 km/s for extended crust (Christensen and Mooney, 1995).

Following the approach of Julià and Mejía (2004), we have estimated formal uncertainties in H and κ by bootstrapping the receiver function data set for each station using 200 replications (Efron and Tibshirani, 1991). The uncertainties for each station using a mean crustal Vp of 6.3 km/s for the H-κ stacking are given in Table 1, along with an overall uncertainty in H obtained by combining the uncertainties obtained using Vp values of 6.3 and 6.5 km/s for the stacking.

Figure 3 shows an example of the H-κ results for station NABD, and Table 1 provides a summary of the results for all of the stations. The H-κ results for the other stations are shown in Figure DR1 in the Data Repository.

DISCUSSION AND CONCLUSIONS

Our results are shown in Figure 4 along with results from several refraction profiles on both margins of the northern Red Sea and seismic stations in Saudi Arabia. Crustal thickness around Lake Aswan (~35–38 km; stations MABD, NNAL, NAHD, and NMAN) is similar to crustal thickness beneath the interior of the Arabian shield, and the crust thins by ~5–10 km toward the coast (27 km beneath station BRNS and 25–26 km beneath stations NABD and HRG). There is some variability in the Vp/Vs ratios between the stations (Table 1), but given their uncertainties they are not significantly different. The average of the ratios (1.78) indicates an intermediate bulk crustal composition.

Crustal thickness from the STEFAN E project refraction profile V (Voggenreiter et al., 1988) shows good agreement near the coast with crustal thickness beneath stations NABD and HRG, but a difference of ~5–8 km in crustal thickness ~150 km inland compared to station BRNS (Fig. 4). We attribute the slightly thinner crust at station BRNS to Late Cretaceous extension and volcanism just to the west of the Red Sea Hills in the South Eastern Desert region (Greiling et al., 1988), and not to Cenozoic rifting in the Red Sea (Fig. 2). An alternative interpretation of the STEFAN E profile V by Makris and Rihm (1991) and Rihm et al. (1991) shows crustal thickness of ~28–30 km beneath the western end of the profile, in comparison to the thicker crust shown in Figure 4 from Voggenreiter et al. (1988).

A comparison of crustal structure on either side of the Red Sea (Fig. 4) reveals similar crustal thicknesses of ~20 km at the coast, 25–32 km beneath stations within ~50 km of the coast, and 35–40 km further inland. Crustal structure beneath the conjugate margins therefore appears to be symmetric, at least within the reported uncertainties of the crustal thickness estimates. What are the implications of this finding for understanding rifting in the northern Red Sea?

Pure shear models of extension (Buck et al., 1988; Cochran, 1983; Martinez and Cochran,

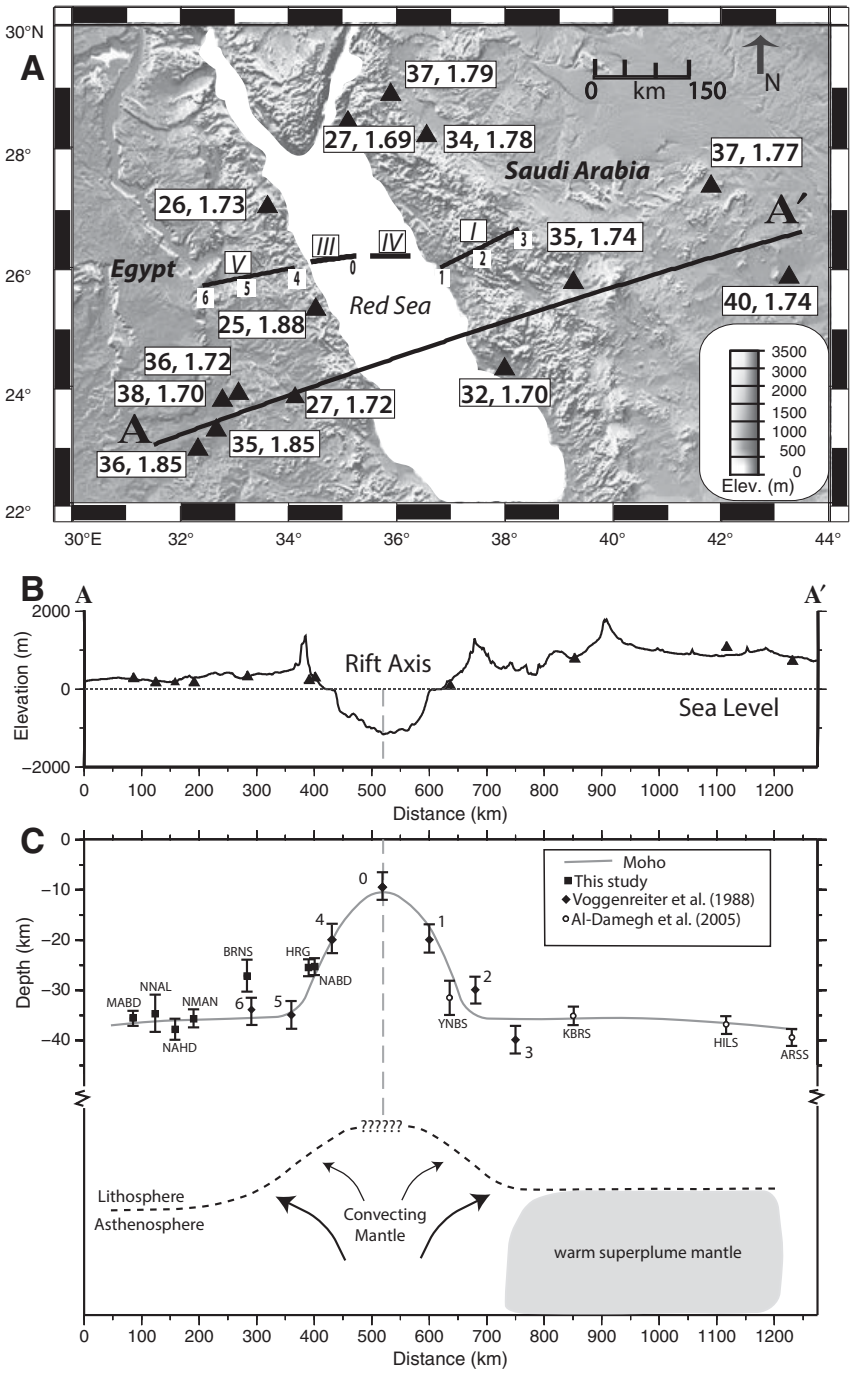

Figure 4. A: Topographic map of northern Red Sea region showing seismic station locations (black triangles) and refraction profiles from STEFAN E project (I–V). Numbers next to seismic stations give crustal thickness (km) and Vp/Vs, and numbers along refraction profiles give locations of crustal thickness estimates shown in C. Elev.—elevation. A-A′ gives location of topographic profile in B. B: Topographic profile across northern Red Sea with location of seismic stations (triangles). C: Crustal thickness estimates projected onto profile A-A′ for seismic stations in Egypt (this study) and Saudi Arabia (Al-Damegh et al., 2005), and from STEFAN E project refraction profiles I–V (Voggenreiter et al., 1988). Solid gray line illustrates symmetric structure of Moho on either side of rift axis. Dashed black line illustrates topography on lithosphere-asthenosphere boundary. Shaded region shows proposed location of warm plume material under eastern margin of Red Sea Rift.

1988) predict symmetric structure across a rift (Fig. 1B), and thus our results, in combination with the other estimates of crustal thickness shown in Figure 4, support such a mode of extension. There is little evidence for asymmetric variations in crustal thickness beneath the conjugate margins, as predicted by simple shear models (Fig. 1A) (Voggenreiter et al., 1988; Bohannon, 1989; Dixon et al., 1989; Rihm et al., 1991) or the pull-apart model of Makris and Rihm (1991). Cochran (2005) noted that the earliest stage of rifting in the northern Red Sea was connected to the Gulf of Suez, where upper crustal structure is asymmetric, but he interpreted the present-day upper crustal morphology across the rift to be symmetric, and suggested that the evolution from asymmetric to symmetric rifting must have occurred late in the rifting process.

Our results showing symmetric crustal thickness beneath the conjugate margins indicate that symmetric thinning of the crust could have begun during the very earliest stages of rifting and not after the development of the Dead Sea transform in the Middle Miocene. In addition, the symmetric crustal structure indicates that the asymmetric uplift and volcanism on the Arabian side of the Red Sea may not be directly related to the rifting process, and instead could be the result of mantle flow from the African superplume (Fig. 4C), as suggested by Daradich et al. (2003) and Hansen et al. (2006).

Pure shear extension in the northern Red Sea, although consistent with models of extension for some rifts (e.g., North Sea, Ziegler, 1992; Rio Grande, Wilson et al., 2005), contrasts with models of simple shear proposed for a number of other rifts (e.g., Galicia, Manatschal and Bernoulli, 1999; Gulf of Mexico, Marion and Buffler, 1993), including the southern Red Sea (Egloff et al., 1991; Voggenreiter et al., 1988). The different modes of extension suggest that rifted margins may develop in different ways, likely reflecting multiple factors that can influence crustal extension, such as preexisting lithospheric structure, extension rates, and the availability of magma, even along strike within one rift system (e.g., the northern versus southern Red Sea).

ACKNOWLEDGMENTS

We thank three anonymous reviewers for helpful reviews. This research has been funded in part by the National Science Foundation (grant OISE-0530062).

REFERENCES CITED

Al-Damegh, K., Sandvol, E., and Barazangi, M., 2005, Crustal structure of the Arabian plate: New constraints from the analysis of teleseismic receiver functions: Earth and Planetary Science Letters, v. 231, p. 177–196, doi:10.1016/j.epsl.2004.12.020.

Bohannon, R.G., 1989, Style of extensional tectonism during rifting: Red Sea and Gulf of Aden: Journal of African Earth Sciences, v. 8, p. 589–602, doi:10.1016/S0899-5362(89)80046-6.

Bosworth, W., Huchon, P., and McCaly, K., 2005, The Red Sea and Gulf of Aden Basins: Journal of African Earth Sciences, v. 43, p. 2334–2378, doi:10.1016/j.jafrearsci.2005.07.020.

Buck, W.R., Martinez, F., Steckler, M.S., and Cochran, J.R., 1988, Thermal consequences of lithospheric extension: Pure and simple: Tectonics, v. 7, p. 213–234, doi:10.1029/TC007i002p00213.

Christensen, N.I., and Mooney, W.D., 1995, Seismic velocity structure and composition of the continental crust, a global view: Journal of Geophysical Research, v. 100, p. 9761–9788, doi:10.1029/95JB00259.

Cochran, J.R., 1983, A model for development of the Red Sea: American Association of Petroleum Geologists Bulletin, v. 67, p. 41–69.

Cochran, J.R., 2005, Northern Red Sea: Nucleation of an oceanic spreading center within a continental rift: Geochemistry, Geophysics, Geosystems, v. 6, Q03006, doi:10.1029/2004GC000826.

Cochran, J.R., Gaulier, J.M., and Le Pichon, X., 1991, Crustal structure and the mechanism of extension in the Northern Red Sea: Constraints from gravity anomalies: Tectonics, v. 10, p. 1018–1037, doi:10.1029/91TC00926.

Coulié, E., Quidelleur, X., Gillot, P.-Y., Courtillot, V., Lefèvre, J.-C., and Chiesa, S., 2003, Comparative K-Ar and Ar/Ar dating of Ethiopian and Yemenite Oligocene volcanism: Implications for timing and duration of the Ethiopian traps: Earth and Planetary Science Letters, v. 206, p. 477–492, doi:10.1016/S0012-821X(02)01089-0.

Daradich, A., Mitrovica, J., Pysklywec, R., Willett, S., and Forte, A., 2003, Mantle flow, dynamic topography and rift flank uplift of Arabia: Geology, v. 31, p. 901–904, doi:10.1130/G19661.1.

Dixon, T.H., Ivins, E.R., and Franklin, B.J., 1989, Topographic and volcanic asymmetry around the Red Sea: Constraints on rift models: Tectonics, v. 8, p. 1193–1216, doi:10.1029/TC008i006p01193.

Efron, B., and Tibshirani, R., 1991, Statistical data analysis in computer age: Science, v. 253, p. 390–395, doi:10.1126/science.253.5018.390.

Egloff, E., Rihm, R., Makris, J., Izzeldyn, Y.A., Bobsien, M., Meier, K., Junge, R., Noman, T., and Warsi, W., 1991, Contrasting styles of the eastern and western margins of the southern Red Sea: The 1988 SONNE experiment: Tectonophysics, v. 198, p. 329–353, doi:10.1016/0040-1951(91)90159-P.

Gaulier, J.M., Le Pichon, X., Lyberis, N., Avedik, F., Geli, L., Moretti, I., Deshamps, A., and Hafez, S., 1988, Seismic study of the crust of the northern Red Sea and Gulf of Suez: Tectonophysics, v. 153, p. 55–88, doi:10.1016/0040-1951(88)90007-8.

Greiling, R.O., El Ramly, L.F., El Akhal, H., and Stem, R.J., 1988, Tectonic evolution of the northern Red Sea margins as related to basement structure: Tectonophysics, v. 153, p. 179–191, doi:10.1016/0040-1951(88)90014-5.

Hansen, S., Schwartz, S., Al-Amri, A., and Rodgers, A., 2006, Combined plate motion and density-driven flow in the asthenosphere beneath Saudi Arabia: Evidence from shear-wave splitting and seismic anisotropy: Geology, v. 34, p. 869–872, doi:10.1130/G22713.1.

Julià, J., and Mejía, J., 2004, Thickness and Vp/Vs ratio variation in the Iberian crust: Geophysical Journal International, v. 156, p. 59–72, doi:10.1111/j.1365-246X.2004.02127.x.

Ligorría, J.P., and Ammon, C.J., 1999, Iterative deconvolution and receiver function estimation: Seismological Society of America Bulletin, v. 89, p. 1395–1400.

Makris, J., and Rihm, R., 1991, Shear-controlled evolution of the Red Sea, pull apart model: Tectonophysics, v. 198, p. 441–466, doi:10.1016/0040-1951(91)90166-P.

Makris, J., Allam, A., Moktar, T., Basahel, A., Dehgani, G.A., and Azari, M., 1983, Crustal structure in the northwestern region of the Arabian Shield and its transition to the Red Sea: Bulletin of the Faculty of Science of King Abdulaziz University, v. 6, p. 435–447.

Manatschal, G., and Bernoulli, D., 1999, Architecture and tectonic evolution of nonvolcanic margins: Present-day Galicia and ancient Adria: Tectonics, v. 18, p. 1099–1119, doi:10.1029/1999TC900041.

Marion, G., and Buffler, R., 1993, Application of simple-shear model to the evolution of passive continental margins of the Gulf of Mexico basin: Geology, v. 21, p. 495–498, doi:10.1130/0091-7613(1993)021<0495:AOSSMT>2.3.CO;2.

Martinez, F., and Cochran, J.R., 1988, Structures and tectonics of the northern Red Sea: Catching a continental margin between rifting and drifting: Tectonophysics, v. 150, p. 1–31, doi:10.1016/0040-1951(88)90293-4.

Omar, G.I., and Steckler, M.S., 1995, Fission track evidence on the initial rifting of the Red Sea: Two pulses, no propagation: Science, v. 270, p. 1341–1344, doi:10.1126/science.270.5240.1341.

Prutkin, I., and Saleh, A., 2009, Gravity and magnetic data inversion for 3D topography of the Moho discontinuity in the northern Red Sea area, Egypt: Journal of Geodynamics, v. 47, p. 237–245, doi:10.1016/j.jog.2008.12.001.

Rihm, R., Makris, J., and Moller, L., 1991, Seismic survey in the northern Red Sea: Asymmetric crustal structure: Tectonophysics, v. 198, p. 279–295, doi:10.1016/0040-1951(91)90156-M.

Sebai, A., Zumbo, V., Féraud, G., Bertrand, H., Hussain, A.G., Giannérini, G., and Campredon, R., 1991, $^{40}Ar/^{39}Ar$ dating of alkaline and tholeiitic magmatism of Saudi Arabia related to the early Red Sea rifting: Earth and Planetary Science Letters, v. 104, p. 473–487, doi:10.1016/0012-821X(91)90223-5.

Voggenreiter, W., Hötzl, H., and Mechie, J., 1988, Low-angle detachment origin for the Red Sea Rift System?: Tectonophysics, v. 150, p. 51–75, doi:10.1016/0040-1951(88)90295-8.

Wilson, R., Aster, R., West, M., Ni, J., Grand, S., Gao, W., Baldridge, W., Semken, S., and Patel, R., 2005, Lithospheric structure of the Rio Grande rift: Nature, v. 433, p. 851–855, doi:10.1038/nature03297.

Zhu, L., and Kanamori, H., 2000, Moho depth variation in southern California from teleseismic receiver functions: Journal of Geophysical Research, v. 105, p. 2969–2980, doi:10.1029/1999JB900322.

Ziegler, P.A., 1992, North Sea rift system: Tectonophysics, v. 208, p. 55–75, doi:10.1016/0040-1951(92)90336-5.

Manuscript received 11 May 2013
Revised manuscript received 30 October 2013
Manuscript accepted 6 November 2013

Printed in USA